AD

TECHNICAL REPORT
75-99-AMEL

THEORETICAL AND EXPERIMENTAL INVESTIGATION OF THE BUCKLING OF RECTANGULAR CYLINDERS

February 1976

Approved for public release;
distribution unlimited.

UNITED STATES ARMY
NATICK DEVELOPMENT CENTER
NATICK, MASSACHUSETTS 01760

Aero-Mechanical Engineering Laboratory

Approved for public release; distribution unlimited.

Citation of trade names in this report does not constitute an official indorsement or approval of the use of such items.

Destroy this report when no longer needed. Do not return it to the originator.

Unclassified

SECURITY CLASSIFICATION OF THIS PAGE (When Data Entered)

REPORT DOCUMENTATION PAGE

READ INSTRUCTIONS BEFORE COMPLETING FORM

1. REPORT NUMBER: Technical Report 75-99-AMEL	2. GOVT ACCESSION NO.
3. RECIPIENT'S CATALOG NUMBER	
4. TITLE (and Subtitle): THEORETICAL AND EXPERIMENTAL INVESTIGATION OF THE BUCKLING OF RECTANGULAR CYLINDERS.	5. TYPE OF REPORT & PERIOD COVERED
	6. PERFORMING ORG. REPORT NUMBER
7. AUTHOR(s): Earl C. Steeves	8. CONTRACT OR GRANT NUMBER(s)
9. PERFORMING ORGANIZATION NAME AND ADDRESS: U.S. Army Natick Development Center, Aero-Mechanical Engineering Laboratory, Natick, Massachusetts 01760	10. PROGRAM ELEMENT, PROJECT, TASK AREA & WORK UNIT NUMBERS: 6.2;1J6627080552;05;017
11. CONTROLLING OFFICE NAME AND ADDRESS: U.S. Army Natick Development Center, Aero-Mechanical Engineering Laboratory, Natick, Massachusetts 01760	12. REPORT DATE: Feb[illegible]1976
	13. NUMBER OF PAGES: 38
14. MONITORING AGENCY NAME & ADDRESS (if different from Controlling Office)	15. SECURITY CLASS. (of this report): Unclassified
	15a. DECLASSIFICATION/DOWNGRADING SCHEDULE

16. DISTRIBUTION STATEMENT (of this Report)

Approved for public release; distribution unlimited

17. DISTRIBUTION STATEMENT (of the abstract entered in Block 20, if different from Report)

18. SUPPLEMENTARY NOTES

19. KEY WORDS (Continue on reverse side if necessary and identify by block number)

CYLINDERS	LOAD CONTROL	CONSTANTS
RECTANGULAR BODIES	LOADING	RATIOS
EQUATIONS	STRESS ANALYSIS	EIGENVALUES
BUCKLING	CONTAINERS	MATRICES
GEOMETRY	PACKAGING	VECTORS (MATHEMATICS)

20. ABSTRACT (Continue on reverse side if necessary and identify by block number)

Classical plate buckling theory is used to model the buckling problem for rectangular cylinders. Solutions to the resulting equations are found directly for the case of a uniformly loaded cylinder and by approximate techniques for the nonuniformly loaded cylinder. Results from a series of experiments to determine the buckling load are presented and compared with predictions from the theory. These comparisons reveal the need to examine geometrically nonlinear buckling problems to more closely model the situation present during the compression loading of rectangular cylinders. In addition, the need to include inelastic behavior for cylinders of low aspect ratio is also revealed.

DD FORM 1 JAN 73 1473 EDITION OF 1 NOV 65 IS OBSOLETE

Unclassified

SECURITY CLASSIFICATION OF THIS PAGE (When Data Entered)

PREFACE

The results presented in this paper were developed during an investigation of the behavior of package and container structures under load. The work was part of a program to formulate a computer-aided design procedure for packaging systems under Task 1J6627080552 05/017, Establishment of Design Criteria for Containers, and 1E662703A090–04 Design, Analysis and Optimization of Structures. This last task was sponsored by the AMC Computer-Aided Design and Engineering Program.

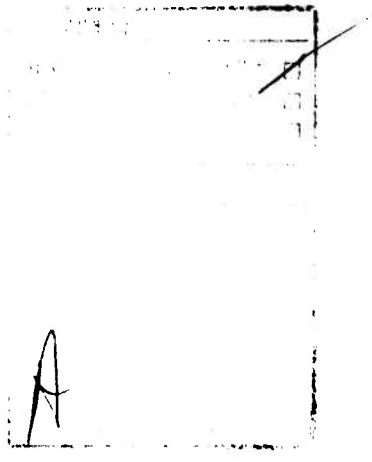

TABLE OF CONTENTS

LIST OF FIGURES

THEORETICAL AND EXPERIMENTAL INVESTIGATION OF THE BUCKLING OF RECTANGULAR CYLINDERS

INTRODUCTION

A review of the package design problem reveals a problem involving many variables and a great quantity of data relative to these variables and the design parameters. The complete design problem involves the interaction of such parameters as shipping route, its associated hazard environment, and characteristics of the item being packaged, such as fragility and cost, with the package and container design parameters. A problem of such complexity is well suited to the computer-aided design approach. One of the requirements for the application of this approach is the ability to specify a package or container design which will protect the contents against the expected shipping, handling, and storage environment. One element of this environment is the load imposed on the package or container and the work reported here is an investigation of the behavior of rectangular packages and containers under one of these loading conditions, namely, the compressive loading due to stacking during shipment or storage.

The stacking problem is treated as the buckling problem for rectangular cylinders subject to axial compression, the objective being to develop a program which would allow specification of a design, given the expected stacking loads. To accomplish this objective, a procedure to compute the buckling loads of rectangular cylinders was developed using the theory of structural mechanics. In addition, tests were conducted to experimentally determine the buckling load of a series of rectangular fiberboard cylinders. Comparison of these experimental results with the computed values provided a measure of the usefulness of the theory. Although the experimental work reported here deals solely with fiberboard cylinders, the theory is applicable to any orthotropic material.

Previous work related to this problem has largely been directed toward developing empirical correlation formulas between the container compressive strength and such properties as ring crush strength, basis weight and Young's Modulus. The results presented in reference 1 typify these efforts in which some of the notions of structural mechanics are utilized but a direct attack on the problem is not made. The most direct attack on the problem known to the author is reported in reference 2. In this work the theory for the buckling of flat plates was utilized to predict the strength of rectangular containers; however, no attempt was made to treat an entire package.

[1] P.E. Shick, and N.C.S. Chan; Top-to-Bottom Compression for Double Wall Corrugated Boxes; TAPPI, Vol 48 No 7; 1965; pp 423-430.

[2] B.S Angell, and P.R. Paslay; Determination of the Stacking Strength of Corrugated Fiberboard Containers; Proceedings of Society of Experimental Stress Analysis, Vol XVI, No 1 pp 109-116.

THEORETICAL PREDICTION OF THE BUCKLING LOAD

The problem to be considered here is that of the strength of a rectangular container under stacking loads. The main load-carrying elements of the container are the four sides which support the load in compression. Because of the compressive load the buckling mode of failure must be considered. To simplify the theoretical treatment of this mode of failure the stacking problem is represented by a rectangular cylinder subjected to axial compression as illustrated in Figure 1. In this section the theoretical aspects and solutions for two approaches to the problem will be presented. The first approach is a direct solution of the governing equations leading to a transcendental eigenvalue problem for the buckling load. The second approach is a finite difference solution which leads to an algebraic eigenvalue problem.

Direct Solution of Governing Equations

Governing Equation and Solution:

The formulation of the problem of the buckling of rectangular cylinders presents some mathematical difficulties because of the discontinuity in the tanget to the cylinder as one proceeds around its perimeter. This difficulty is overcome by treating each of the four sides of the cylinder as flat plates, as shown in Figure 2, and accounting for the interaction of the sides through boundary conditions expressing continuity of displacement and equilibrium of moments at the corners. To accomplish this a coordinate system is established on each of the sides as shown in Figure 2. The equations governing the buckling of each of the plates subject to an axial compressive stress N_x are:

$$D_{11}\frac{\partial^4 w_i}{\partial x^4} + 2(D_{12}+2D_{33})\frac{\partial^4 w_i}{\partial x^2 \partial y_i^2} + D_{22}\frac{\partial^4 w_i}{\partial y_i^4} - N_x\frac{\partial^2 w_i}{\partial x^2} = 0 \qquad (1)$$

A complete development of these equations, which are written for an orthotropic plate whose principal directions are parallel with the x_1, y_1 directions, is given in reference 3. In equation (1) i takes on the values 1-4 giving an equation for each plate. This equation is nondimensionalized by dividing by D_{11} and letting $x=a\xi$ and $y_i=a\eta_i$:

$$\frac{\partial^4 w_i}{\partial \xi^4} + 2e_1\frac{\partial^4 w_i}{\partial \xi^2 \partial \eta_i^2} + e_2\frac{\partial^4 w_i}{\partial \eta_i^4} + N\frac{\partial^2 w_i}{\partial \xi^2} = 0 \qquad (2a)$$

$$e_1 = \frac{D_{12}}{D_{11}} + 2\frac{D_{33}}{D_{11}} \qquad (2b)$$

$$e_2 = \frac{D_{22}}{D_{11}} \qquad (2c)$$

$$N = \frac{N_x a^2}{D_{11}} \qquad (2d)$$

[3] R.F.S. Hearmon; An Introduction To Applied Anisotropic Elasticity; Oxford University Press; 1961.

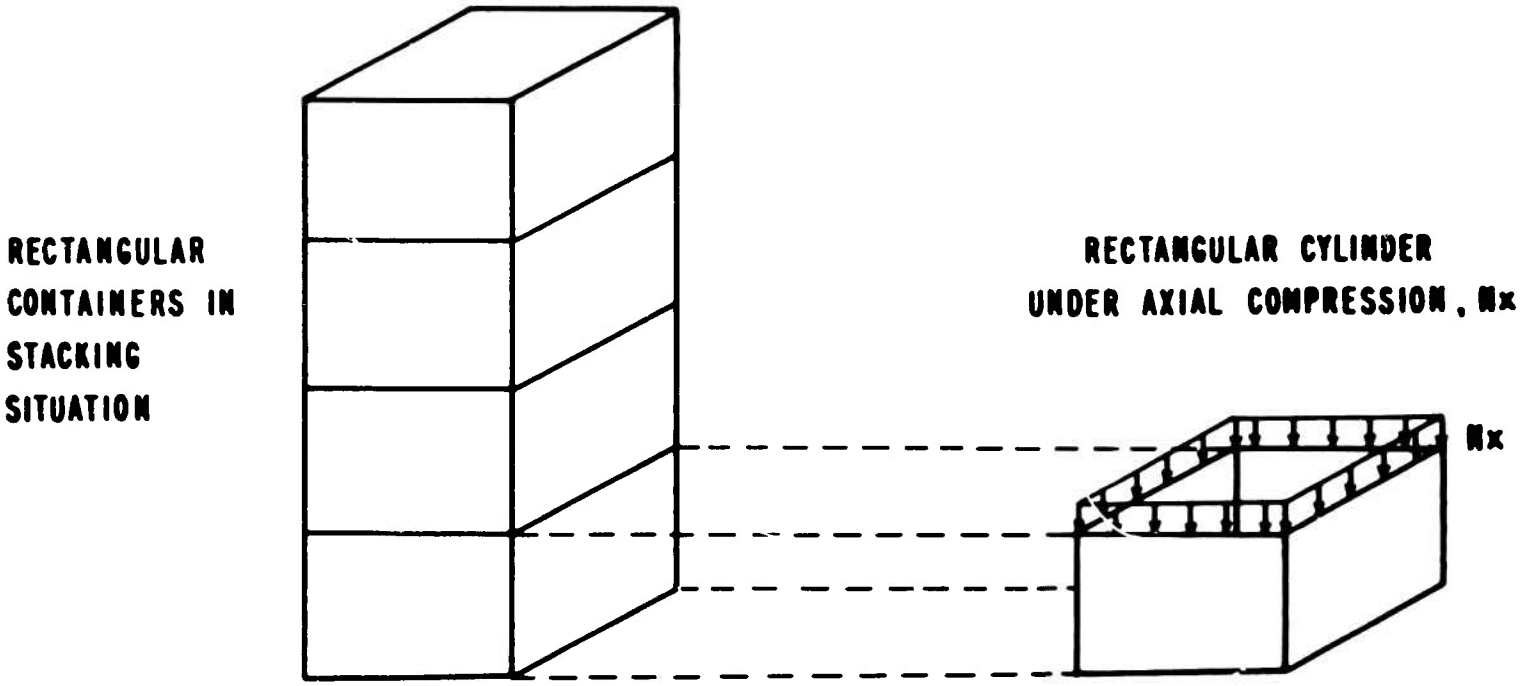

Figure 1 Model used for analysis of stacking loads on rectangular container

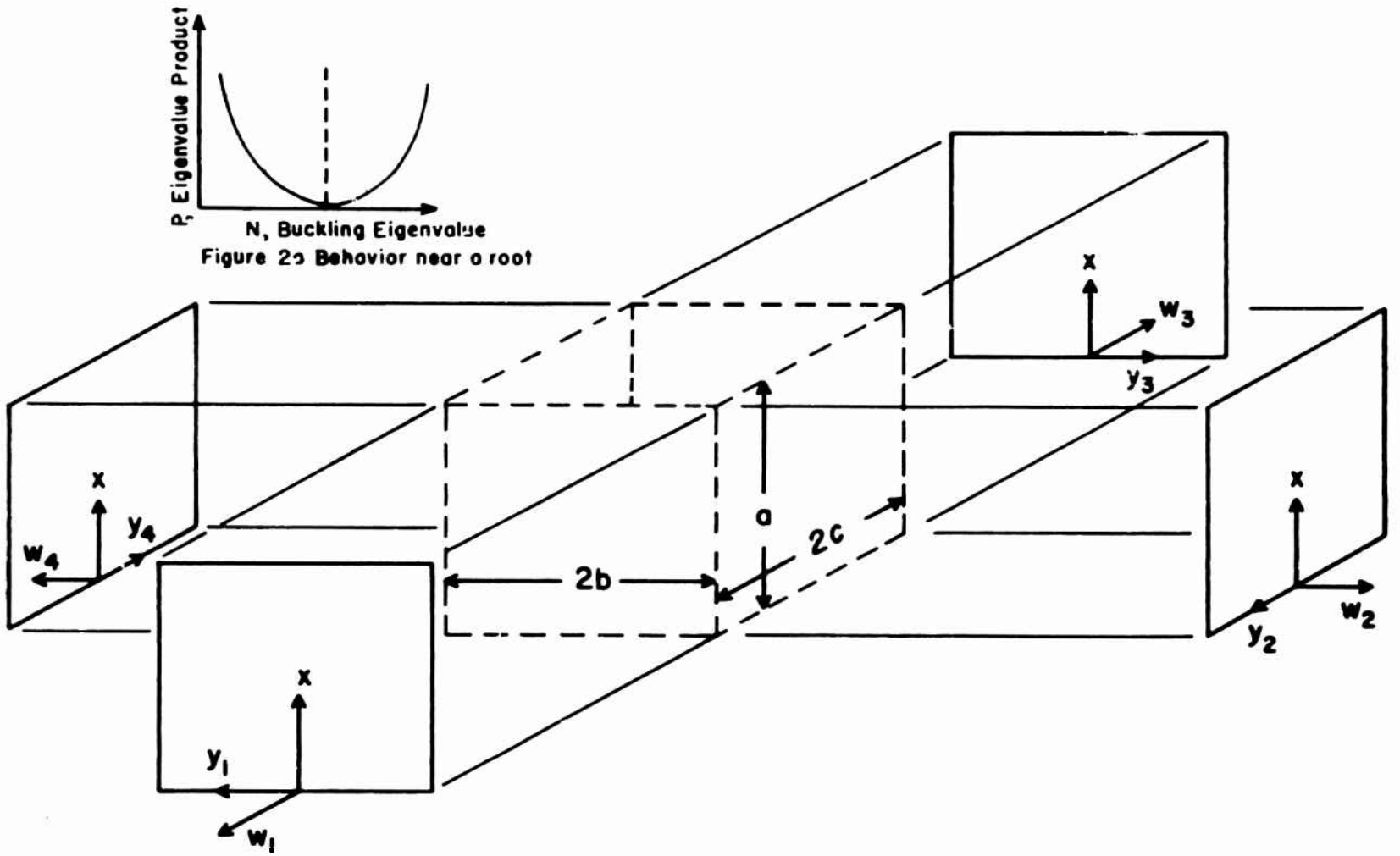

Figure 2b Behavior near a root

Figure 2 Coordinate Systems used in Analysis of Rectangular Cylinder

In writing equation (2) account has been taken of the compressive nature of N_x by changing the sign of the term containing this parameter. It is assumed that the boundaries $\xi=0$ and $\xi=1$ are simply supported, that is, the displacement and the moment vanish at these boundaries. With this assumption the normal displacements w_i are expressed as:

$$w_i(\xi,\eta_i) = F_i(\eta_i)\ \mathrm{Sin}\ n\pi\xi \tag{3}$$

and equation (2) is reduced to

$$(n\pi)^4 F_i - 2e_1(n\pi)^2 \frac{d^2F_i}{d\eta_i^2} + e_2 \frac{d^4F_i}{d\eta_i^4} - N(n\pi)^2 F_i = 0 \tag{4}$$

The solution of this equation is

$$F_i(\eta_i) = A_i\mathrm{Sinh}\alpha\eta_i + B_i\mathrm{Cosh}\alpha\eta_i + C_i\mathrm{Sin}\beta\eta_i + D_i\mathrm{Cos}\beta\eta_i \tag{5}$$

where

$$\alpha = n\pi\sqrt{\frac{e_1}{e_2} + \sqrt{\left(\frac{e_1}{e_2}\right)^2 + \frac{1}{e_2}\left(\frac{N}{(n\pi)^2} - 1\right)}} \tag{6a}$$

$$\beta = n\pi\sqrt{-\frac{e_1}{e_2} + \sqrt{\left(\frac{e_1}{e_2}\right)^2 + \frac{1}{e_2}\left(\frac{N}{(n\pi)^2} - 1\right)}} \tag{6b}$$

This gives the complete solution as

$$w_i = \mathrm{Sin}(n\pi\xi)\ \left[A_i\mathrm{Sinh}(\alpha\eta_i) + B_i\mathrm{Cosh}(\alpha\eta_i) + C_i\mathrm{Sin}(\beta\eta_i) + D_i\mathrm{Cos}(\beta\eta_i)\right] \tag{7}$$

With the constants of integration and the buckling eigenvalue to be determined by application of the conditions joining the corners.

Joining Constraints:

The developments up to this point have considered the sides of the rectangular cylinder as though they were not joined. In order to complete the solution it is necessary to state the conditions joining the sides and apply these conditions to the solution obtained above.

Because of the relatively greater inplane stiffness of the plates it is assumed that at each corner the normal displacement vanishes; this is expressed mathematically as:

$$w_1(\xi, b/a) = 0 \qquad w_3(\xi, b/a) = 0$$

$$w_1(\xi, -b/a) = 0 \qquad w_3(\xi, -b/a) = 0$$

$$w_2(\xi, c/a) = 0 \qquad w_4(\xi, c/a) = 0 \tag{3}$$

$$w_2(\xi, -c/a) = 0 \qquad w_4(\xi, -c/a) = 0$$

Equations (8) must be satisfied for all ξ.

Application of these conditions to the solution allows the determination of eight of the sixteen constants in equation (7) yielding the following for the solution:

$$w_1 = C_1[\mathrm{Sin}(\beta\eta_1) + f_2\mathrm{Sinh}(\alpha\eta_1)] + D_1[\mathrm{Cos}(\beta\eta_1) + f_1\mathrm{Cosh}(\alpha\eta_1)] \mathrm{Sin}(n\pi\xi)$$

$$w_2 = C_2[\mathrm{Sin}(\beta\eta_2) + f_4\mathrm{Sinh}(\alpha\eta_2)] + D_2[\mathrm{Cos}(\beta\eta_2) + f_3\mathrm{Cosh}(\alpha\eta_2)] \mathrm{Sin}(n\pi\xi)$$

$$w_3 = C_3[\mathrm{Sin}(\beta\eta_3) + f_2\mathrm{Sinh}(\alpha\eta_3)] + D_3[\mathrm{Cos}(\beta\eta_3) + f_1\mathrm{Cosh}(\alpha\eta_3)] \mathrm{Sin}(n\pi\xi) \tag{9}$$

$$w_4 = C_4[\mathrm{Sin}(\beta\eta_4) + f_4\mathrm{Sinh}(\alpha\eta_4)] + D_4[\mathrm{Cos}(\beta\eta_4) + f_3\mathrm{Cosh}(\alpha\eta_4)] \mathrm{Sin}(n\pi\xi)$$

In equation (9) the constants f_i have the following definition:

$$f_1 = -\mathrm{Cos}(\beta b/a)/\mathrm{Cosh}(\alpha b/a)$$

$$f_2 = -\mathrm{Sin}(\beta b/a)/\mathrm{Sinh}(\alpha b/a)$$

$$f_3 = -\mathrm{Cos}(\beta c/a)/\mathrm{Cosh}(\alpha c/a) \tag{10}$$

$$f_4 = -\mathrm{Sin}(\beta c/a)/\mathrm{Sinh}(\alpha c/a)$$

The remaining eight joining conditions to be applied express the continuity of first and second derivatives of the displacements at the corners as:

$$w_1'(\xi, -b/a) - w_2'(\xi, c/a) = 0$$

$$-w_1''(\xi, -b/a) + w_2''(\xi, c/a) = 0 \tag{11}$$

$$
\begin{aligned}
w_2'(\xi, -c/a) - w_3(\xi, b/a) &= 0 \\
-w_2''(\xi, -c/a) + w_3'(\xi, b/a) &= 0 \\
w_3(\xi, -b/a) - w_4(\xi, c/a) &= 0 \\
-w_3'(\xi, -b/a) + w_4'(\xi, c/a) &= 0 \\
w_4(\xi, -c/a) - w_1(\xi, b/a) &= 0 \\
-w_4''(\xi, -c/a) + w_1''(\xi, b/a) &= 0
\end{aligned}
\tag{11}
$$

for all ξ.

Where the primes denote differentiation with respect to the appropriate variable. Substitution of equations (9) into (11) yields the following set of homogenous equations written in matrix form:

$$[U] \{c\} = 0 \tag{12}$$

In equation (12) $\{c\}$ is a vector whose elements are the constants C_1, D_1, C_2, D_2, C_3, D_3, C_4, D_4 and the nonvanishing elements of the matrix $[U]$, which is of order 8, are given in Appendix I.

A non-trivial $\{c\}$ which satisfies equation (12) exists only if the matrix U is singular; thus one seeks the values of N which cause U to be singular and the corresponding solution. These are respectively the buckling eigenvalue and buckling mode shape.

Extraction of Buckling Eigenvalues:

As indicated above, the values of N which cause the matrix U to be singular are sought; however, the parameter N appears transcendentally in the elements of U so a direct attack is not possible and a search and interpolation scheme must be used. The scheme used to obtain the results presented in this report is based on the theorem presented and proved in reference 4 which deals with the solution of sets of homogenous equations in which one or more of the equations are redundant. The results presented in reference 4 are motivated by the situation in which the number of equations is less than the number of unknowns; however, the extension to the present case is straightforward.

[4]W.C. Walton, Jr., and E.C. Steeves; A New Matrix Theorem and Its Application for Establishing Independent Coordinates for Complex Dynamical Systems with Constraints; NASA TR-R-326; 1969.

According to the theorem proven in reference 4, the solution of a system of homogenous equations like (12) can be expressed as a linear combination of the eigenvectors corresponding to the eigenvalues of the product matrix U^TU having the value zero. When the matrix U is square and nonsingular U^TU will have no zero eigenvalues and equation (12) will have no non-trivial solution. Thus determination of the buckling eigenvalues is reduced to finding the value of N which causes one of the eigenvalues of U^TU to vanish. The fact that the singularity of U will cause one of the eigenvalues of U^TU to vanish results from the fact the singularity implies a redundant equation, and it is shown in reference 4 that a redundant equation manifests itself in a vanishing eigenvalue of U^TU. It should be noted that although U is square, it is not symmetric; because of this a procedure based on the eigenvalues of U was not adopted because of the question of realness of eigenvalues that arise with nonsymmetric matrices The search aspect of the solution scheme is carried out by computing the product of the eigenvalues of U^TU for successive values of N until a value of N close to the solution is found. Because the product matrix U^TU is positive semi-definite the eigenvalues are always greater than or equal to zero. Thus the product of the eigenvalues is greater than or equal to zero giving the behavior of the product of the eigenvalues as a function of N near a solution as shown in Figure 2a. The usual technique of looking for a change in sign to detect nearness to a solution is not applicable in this case and the alternate procedure of looking for changes in the sign of the difference of successive values of the eigenvalue product is used. This is, in effect, looking for changes in the slope of the function shown in Figure 2a. Once the location of a root is found through this search procedure an interpolation procedure is used to find the value of the root to within a specified degree of accuracy. A quadratic interpolation is used because of the behavior near the root. When a root has been located three pairs of values (N, P) where P is the product of the eigenvalues of U^TU, are known and are used to determine a quadratic function. The next trial value of N is that value which causes the slope of this quadratic function to vanish. Using this value of N the corresponding value of P is computed, and this (N, P) pair is used in conjunction with the two most recent pairs to obtain a new quadratic interpolation function which yields a new trial-value of N. This interpolation procedure is continued until the normalized difference between two successively computed values of N is less than a specified convergence criterion.

Two questions arise regarding the use of this technique for finding the roots. The first concerns the behavior when the matrix U is poorly conditioned, that is, when the determinant of U approaches the value zero for values of N not near a solution. In such a case

$$\text{Det. } U \cong \epsilon$$

where

$$\epsilon < 1$$

The present technique utilizes the matrix U^TU for which the determinant in the case of a poorly conditioned matrix is

$$\text{Det } U^TU \cong \epsilon^2$$

Thus, in comparison to the commonly used techniques based on the determinate of U, the present technique is more prone to conditioning problems because of the above quadratic dependence on ϵ. This problem was not encountered in any of the computations carried out in this work indicating that the equations expressed are clearly linearly independent. The second question concerns the possible detection of false solutions. Such false solutions correspond to values of N for which the slope vanishes with a non-zero value for the product of eigenvalues. No automatic procedure was developed to rule out this possibility but in each case the eigenvalues corresponding to a solution were examined to verify that at least one of them vanished. Because of round-off it is necessary to examine the eigenvalues as opposed to their product.

Results using this technique are presented in a subsequent section of this report.

Finite Difference Solution

The direct solution of governing equations described in the preceding section is computationally inefficient because of the indirect approach to eigenvalue extraction and is limited to the treatment of uniformly loaded cylinders. In an effort to improve computational efficiency and develop a method capable of treating nonuniformly loaded rectangular cylinders, an approximate solution based on finite difference procedures was developed.

Energy Minimization Procedure:

Although finite difference procedures are generally applied directly to differential equations, it is possible to use this approximation technique to reduce an integral energy minimization principle to a system of algebraic equations without first developing the differential equations as is described in reference 5 for the plate vibration problem. This procedure, slightly modified, is used here for the buckling of rectangular cylinders.

The energy principle from which the governing equation (2) can be derived is the minimization of the following integral.

[5]W.C. Walton, Jr.; Application of a General Finite Difference Method for Calculating Bending Deformations of Solid Plates; NASA TN D-536; 1960.

$$\iint \frac{1}{2}\left\{D_{11}\left(\frac{\partial^2\bar{w}}{\partial x^2}\right)^2 + 2D_{12}\left(\frac{\partial^2\bar{w}}{\partial x^2}\right)\left(\frac{\partial^2\bar{w}}{\partial y^2}\right) + D_{22}\left(\frac{\partial^2\bar{w}}{\partial y^2}\right)^2 + 4D_{33}\left(\frac{\partial^2\bar{w}}{\partial x\partial y}\right)^2 + Nx\left(\frac{\partial\bar{w}}{\partial x}\right)^2\right\}dxdy \tag{13}$$

The origin of the coordinates y_i and thus η_i has been shifted from the center of the sides to the corner of the cylinder for this finite difference analysis. The geometrical symmetry of the rectangular cylinder makes it possible to treat only one-quarter of the cylinder, as shown in Figure 3, where the coordinate system to be used is also shown. Here, as in the previous analysis, initially the sides are treated as though they are not attached; thus the energy is written in nondimensional form as:

$$\int_0^{b/a}\int_0^1 \frac{1}{2}\left\{\left(\frac{\partial^2\bar{w}}{\partial\xi^2}\right)^2 + 2e_3\left(\frac{\partial^2\bar{w}_1}{\partial\xi^2}\right)\left(\frac{\partial^2\bar{w}_1}{\partial\eta_1^2}\right) + e_2\left(\frac{\partial^2\bar{w}_1}{\partial\eta_1^2}\right)^2 + 4e_4\left(\frac{\partial^2\bar{w}_1}{\partial\xi\partial\eta_1}\right)^2 + N\left(\frac{\partial\bar{w}_1}{\partial\xi}\right)^2\right\}d\xi d\eta_1 + \int_0^{c/a}\int_0^1 \left\{\frac{1}{2}\left(\frac{\partial^2\bar{w}_2}{\partial\xi^2}\right) + 2e_3\left(\frac{\partial^2\bar{w}_2}{\partial\xi^2}\right)\left(\frac{\partial^2\bar{w}_2}{\partial\eta_2^2}\right) + e_2\left(\frac{\partial^2\bar{w}_2}{\partial\eta_2^2}\right)^2 + 4e_4\left(\frac{\partial^2\bar{w}_2}{\partial\xi\partial\eta_2}\right)^2 + N\left(\frac{\partial\bar{w}_2}{\partial\xi}\right)^2\right\}d\xi d\eta_2 \tag{14}$$

where $e_3 = D_{12}/D_{11}$ and $e_4 = D_{33}/D_{11}$ and the other parameters are as previously defined. The assumption of simply supported ends at x=0 and x=a allows specification of $\bar{w}_1$ and $\bar{w}_2$ as

$$\bar{w}_1(\xi, \eta_1) = w_1(\eta_1)\mathrm{Sin}(n\pi\xi)$$
$$\bar{w}_2(\xi, \eta_2) = w_2(\eta_2)\mathrm{Sin}(n\pi\xi) \tag{15}$$

Subsitution of these expressions into the energy and carrying out the integration with respect to ξ transforms (14) to the following one-dimensional energy expression

$$\int_0^{b/a} \frac{1}{2}E d\eta_1 + \int_0^{c/a} \frac{1}{2}E d\eta_2 \tag{16}$$

where

$$E = \left(\frac{n\pi}{2}\right)^4 (w_1)^2 - 2\,\frac{e_3(n\pi)^2}{2}(w_1)\left(\frac{d^2w_1}{d\eta_1^2}\right) + \frac{e_2}{2}\left(\frac{d^2w_1}{d\eta_1^2}\right)^2 + 4\,\frac{e_4(n\pi)^2}{2}\left(\frac{dw_1}{d\eta_1}\right)^2 + \frac{N(n\pi)^2}{2}w_1^2 \tag{17}$$

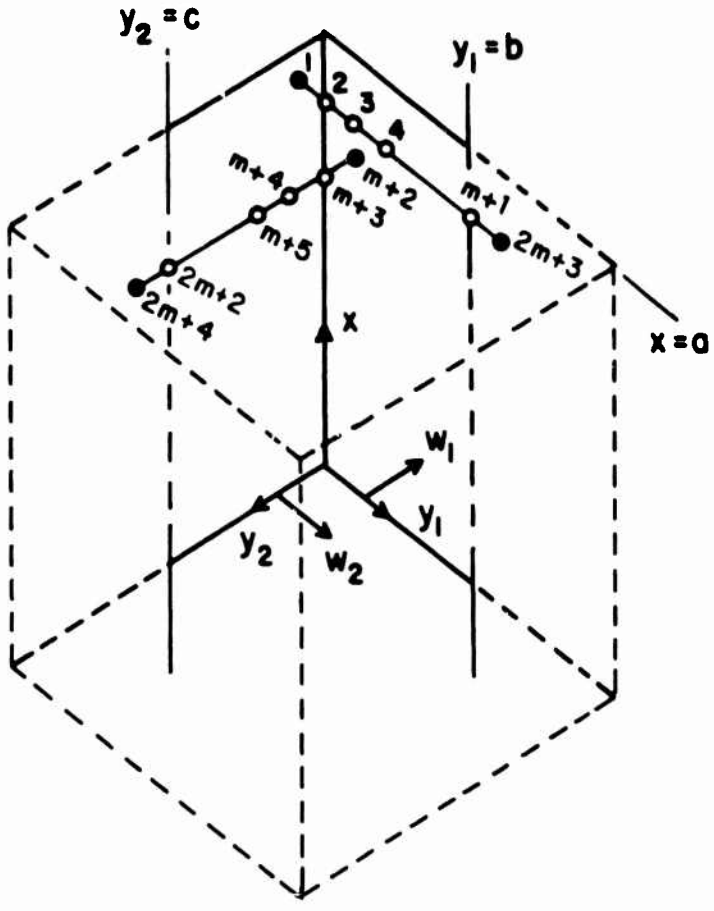

Figure 3 Coordinate System and Finite Difference Grid

over $0 \leq \eta_1 \leq b/a$ with a similar expression over $0 \leq \eta_2 \leq c/a$ and with w_1 and η_1 replaced respectively by w_2 and η_2.

Reduction to Algebraic Eigenvalue Problem:

To carry out the reduction of equation (16) to an algebraic eigenvalue problem using finite difference procedures, a grid is established as shown in Figure 3. In this figure grid points on the structure are denoted by open symbols, and the grid points not on the structure required for evaluation of derivatives at the boundary points are denoted by solid symbols.

On each side m grid points are used; these are numbered 2 through (m+1) on $0 \leq y_1 \leq b$ and (m+3) through (2m+2) on $0 \leq y_2 \leq C$. The four off-structure points are numbered 1, (m+2), (2m+3), (2m+4). The first step in the reduction is the evaluation of the integrals in equation (16) in terms of the energy density function E evaluated at the grid points. This is accomplished using Simpson's Rule for integration and the expression for the energy (16) becomes:

$$\frac{1}{2}\left\{[E_2 + 4E_3 + 2E_4 + 4E_5 + \cdots 2E_{m-1} + 4E_m + E_{m+1}]\ \frac{\Delta\eta_1}{3}\right.$$

$$\left. + [E_{m+3} + 4E_{m+4} + 2E_{m+5} + 4E_{m+6} + \cdots 2E_{2m} + 4E_{2m+1} + E_{2m+2}]\right\} \frac{\Delta\eta_2}{3} \quad (18)$$

$\Delta\eta_i$ is the grid point spacing.

To complete the reduction to an algebraic eigenvalue problem the energy density function E_i at any point is expressed in terms of the grid point displacements w_i by using finite difference approximations for the derivatives in equation (17) to give:

$$E_i = (n\pi)^4 (w_i)^2 - 2e_3(n\pi)^2 (w_i) \frac{w_{i-1}-2w_i+w_{i+1}}{\Delta\eta_1^2} + e_2 \frac{(w_{i-1}-2w_i+w_{i+1})^2}{\Delta\eta_1^4}$$

$$+ 4e_4 (n\pi)^2 \frac{(w_{i-1}+w_{i+1})^2}{4\Delta\eta_1^2} + N(n\pi)^2 w_i^2 \quad (19)$$

for i = 2 to (m+1) and a similar expression for i = (m+3) to (2m+2) with $\Delta\eta_1$ replaced with $\Delta\eta_2$. The quadratic expression (19) can be written in matrix form as

$$E_i = \begin{Bmatrix} w_{i-1} \\ w_i \\ w_{i+1} \end{Bmatrix}^T \left\langle \begin{bmatrix} a_1 & a_2 & a_3 \\ a_2 & a_4 & a_5 \\ a_3 & a_5 & a_6 \end{bmatrix} + \begin{bmatrix} 0 & 0 & 0 \\ 0 & Nd_i & 0 \\ 0 & 0 & 0 \end{bmatrix} \right\rangle \begin{Bmatrix} w_{i-1} \\ w_i \\ w_{i+1} \end{Bmatrix} \tag{20}$$

where a_j j=1,6 and d_i are given in Appendix II. Substitution of these expressions into equation (18) yields the following matrix expression for the total energy:

$$\{w\}^T [S] \{w\} + N \{w\}^T [T] \{w\} \tag{21}$$

w is a vector whose elements are the grid point displacements w_i and [S] and [T] are matrices constructed from the 3 X 3 matrices in equation (20). The elements of these 3 X 3 matrices are given in Appendix II.

Application of Constraints:

Before the energy (21) can be minimized to yield the equilibrium equations, the constraints which express the symmetry conditions and the conditions which join the sides of the cylinder must be imposed. This is accomplished through a direct application of the procedure described in reference 4.

From the results of the direct solution it was known that the lowest buckling eigenvalue for this problem is associated with a deformation shape in which all sides undergo symmetric deformation. Thus the symmetry conditions at η_1=b/a and η_2=c/a are the vanishing of the slopes at these points. These constraints can be expressed mathematically in terms of the finite difference approximations as

$$w_{2m+3} - w_m = 0$$

$$w_{2m+4} - w_{2m+1} = 0 \tag{22}$$

The constraints required to impose the joining of the sides are the vanishing of the normal displacements at η_1=0 and η_2=0 and the continuity of the slope and curvature of the corner. These are expressed in finite difference form as:

$$w_2 = 0$$
$$w_{m+3} = 0$$
$$1/2\Delta\eta_1 (w_3 - w_1) - 1/2\Delta\eta_2 (w_{m+4} - w_{m+2}) = 0$$
$$1/\Delta\eta_1^2 (w_1 - 2w_2 + w_3) + 1/\Delta\eta_2^2 (w_{m+2} - 2w_{m+3} + w_{m+4}) \tag{23}$$

These six homogenous equations (22) and (23) can be expressed in matrix form as

$$[C]\{w\} = 0 \tag{24}$$

where [C] is a 6X(2m+4) matrix whose non-vanishing elements are given in Appendix III. The procedure in reference 4 provides a transformation of the vector $\{w\}$ into a new vector of generalized coordinates $\{q\}$ which satisfy equation (24) and are expressed in the form

$$w = [\beta]\{q\} \tag{25}$$

This transformation is used in equation (21) to give an expression for the energy in terms of generalized coordinates which obey the symmetry and joining constraints

$$\{q\}^T [\bar{S}] \{q\} + N \{q\}^T [\bar{T}] \{q\} \tag{26}$$

where

$$[\bar{S}] = [\beta]^T [S] [\beta]$$

$$[\bar{T}] = [\beta]^T [T] [\beta] \tag{27}$$

Minimization of the energy with respect to the generalized coordinates $\{q\}$ yields the following equilibrium equations:

$$[\bar{S}]\{q\} + N [\bar{T}] \{q\} = 0 \tag{28}$$

Solutions to these equations were obtained by the use of the threshold Jacobi Numerical Technique. Once the eigenvalue N and the corresponding eigenvectors [Q] are obtained, the eigenvectors can be transformed back to the physical coordinates $\{w\}$ by the use of equation (25).

Treatment of Nonuniform Load:

To this point the development of the finite difference solution has considered the uniformly loaded cylinder. The geometry of the rectangular cylinder suggested that the treatment of the nonuniform loads might be required.

A nonuniform load implies that the parameter N in equation (14) is not a constant but a function of η_1 and η_2. This has the principal effect of modifying the matrix element d_i in equation (20) and the interpretation of the buckling eigenvalue N. The types of load distribution of interest are those in which a greater portion of the load

is supported at the corners as illustrated in Figure 4. Such a distribution is conveniently modeled by two second order polynominals. In choosing the exact form for these polynomials, it is desirable to place certain constraints on their behavior, namely, they must be continuous at the corner, take on their minima at $\eta_1 = b/a$ and $\eta_2 = c/a$ and be symmetrical about these points. Functions satisfying these constraints are:

$$N = \bar{N} \left\{ 1 + b_1 \left(\frac{c/a}{b/a} \right)^2 [(\eta_1 - b/a)^2 - 1/3(b/a)^2] \right\} \quad \text{on } 0 \leq \eta_1 \leq b/a$$

$$N = \bar{N} \left\{ 1 + b_1 [(\eta_1 - c/a)^2 + 1/3(c/a)^2] \right\} \quad \text{on } 0 \leq \eta_2 \leq c/a \qquad (29)$$

The parameter $\bar{N}$, which will be the eigenvalue found by the solution, is the average value of the buckling stress; its product with the perimeter gives the total load applied to the cylinder as is the case with the eigenvalue associated with the uniform load. This facilitates comparison of the results from the two loading conditions, since they are both proportional to the total load-carrying capability of the cylinder. The factor b_1 appearing in the expression for the buckling stress (29) is specified so that the ratio of the maximum value of N to its minimum value takes on the desired value.

The changes in the functional form of the buckling stress distribution described above changes the element of the matrix [T] in equation (21), or more specifically, it changes the formula used to compute d_i in equation (20). The formulas to be used in this case are presented in Appendix II. The form of the equation to be solved (28) remains unchanged; however, the elements of $[\bar{T}]$ are changed and the interpretation of the eigenvalue $\bar{N}$ becomes that of the average buckling stress.

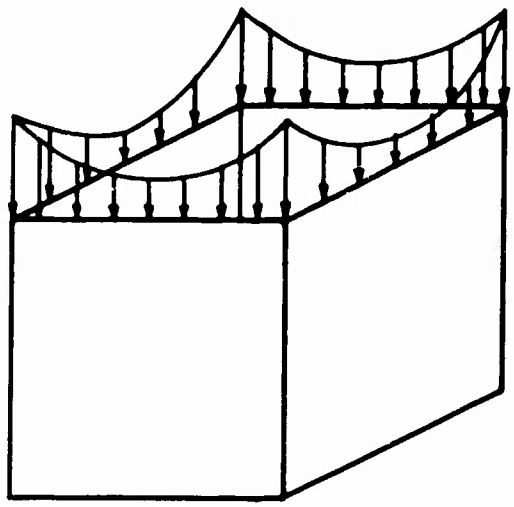

Figure 4 Illustration of the nonuniform load distribution

EXPERIMENTAL DETERMINATION OF THE BUCKLING LOAD

The validity and range of application of the theoretical solutions presented in the previous sections can be established by correlation with experimental results. To make this possible, a series of rectangular fiberboard cylinders were tested to produce a body of experimental data with which the theoretical predictions could be compared. The experimental procedures used are described here.

Each specimen was fabricated in the form of a rectangular cylinder; that is, a rectangular container with no top or bottom flaps, from V3C grade corrugated fiberboard with the corrugations running parallel to the cylinder axis. Each of the cylinders had a stapled lap seam in one corner parallel to the axis of the cylinder. The sizes of the cylinders can be expressed by the two aspect ratios b/a and c/a and magnitude of the cylinder height a. The aspect ratios of the specimens tested ranged from 0.2 to 0.8 with cylinder heights of 0.457, 0.609 and 0.762 m included.

The buckling tests were carried out on a Tinius Olsen testing machine capable of accepting the large specimens involved in this testing program. A photograph of this testing machine with a specimen in position is shown in Figure 5.

The tests were conducted by loading the specimen starting at the unloaded state and increasing the load at a uniform rate of 1.0 cm/min. Loading was continued until deformation of the specimen occurred with no further increase in load. The buckling load was taken to be the maximum load reached as measured on the Tinius Olsen load-measuring system. The total load was reduced to a buckling stress by dividing this buckling load by the perimeter of the cylinder. For each size cylinder two tests were performed.

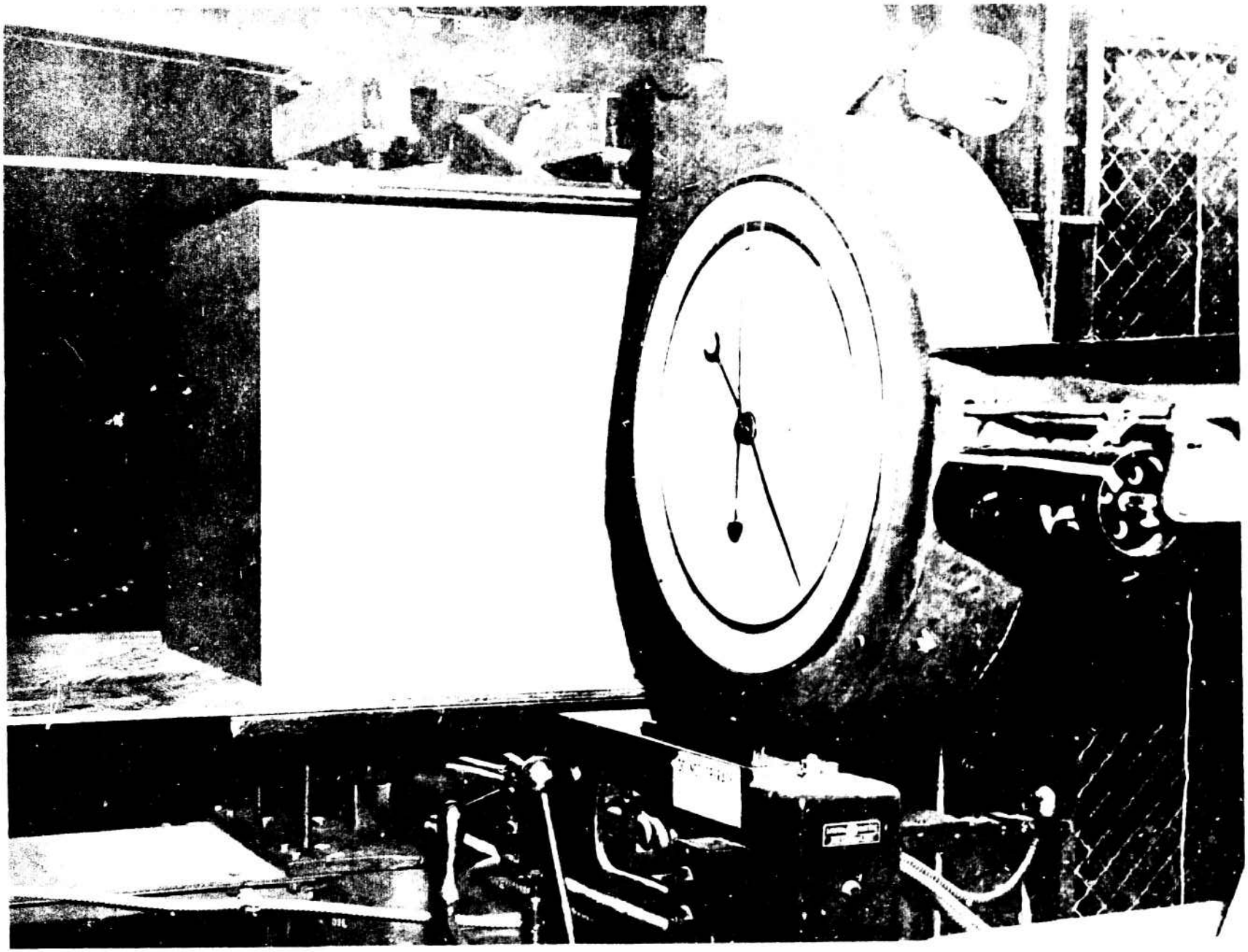

FIGURE 5. Rectangular Cylinder on Testing Machine

RESULTS

The presentation of the results will begin with a discussion of the experimental behavior of the buckling stress as a function of cylinder geometry and follow with a discussion of the theoretical predictions and a comparison of these predictions with the experimental behavior. The section will include the discussion of the validity of the theory and some suggestions for its modification.

Experimental Results

The graphs in Figures 6 and 7 illustrate the behavior of the buckling stress as a function of aspect ratio and cylinder height. In both figures the nondimensional buckling stress is plotted as a function of aspect ratio, b/a. The buckling stress is nondimensionalized according to equation (2) with D_{11} = 14.77 N-m, as given in reference 6. In Figure 6 results are given for two values of the other aspect ratio, c/a, with the cylinder height constant; while in Figure 7 results are given for three values of cylinder height with the aspect ratio, c/a, held constant. The results in Figure 6 show that the buckling stress increases with decreases in either of the aspect ratios. Thus, for buckling failure a rectangular cylinder becomes stronger as the width of the sides become smaller in comparison to the height.

A similar behavior with respect to aspect ratio b/a is seen from the results in Figure 7. Additionally, it is seen that the buckling stress decreases with the cylinder height. This is an unexpected result. The nondimensional governing equations and boundary conditions contain the nondimensional buckling stress and the aspect ratios, thus since the cylinder height, a, does not appear explicitly one would expect the nondimensional buckling stress to be independent of cylinder height. That is, that the nondimensional buckling stress be completely specified by the aspect ratios c/a and b/a for all values of a. As a result one expects the total dependence of the physical buckling stress, N_x, on the cylinder sizes as measured by the cylinder height, a, to be expressed in the definition of the nondimensional buckling stress:

$$N = \frac{N_x a^2}{D_{11}}$$

Since one would expect that N would be independent of "a" the experimental behavior illustrated in Figure 7 then suggests some inadequacy in the theory which will be discussed subsequently in connection with the comparison of theoretical and experimental results.

[6]E.C. Steeves; Orthotropic Bending Properties of Fiberboard, Technical Report 75-97-AMEL; U.S. Army Natick Development Center; 1975.

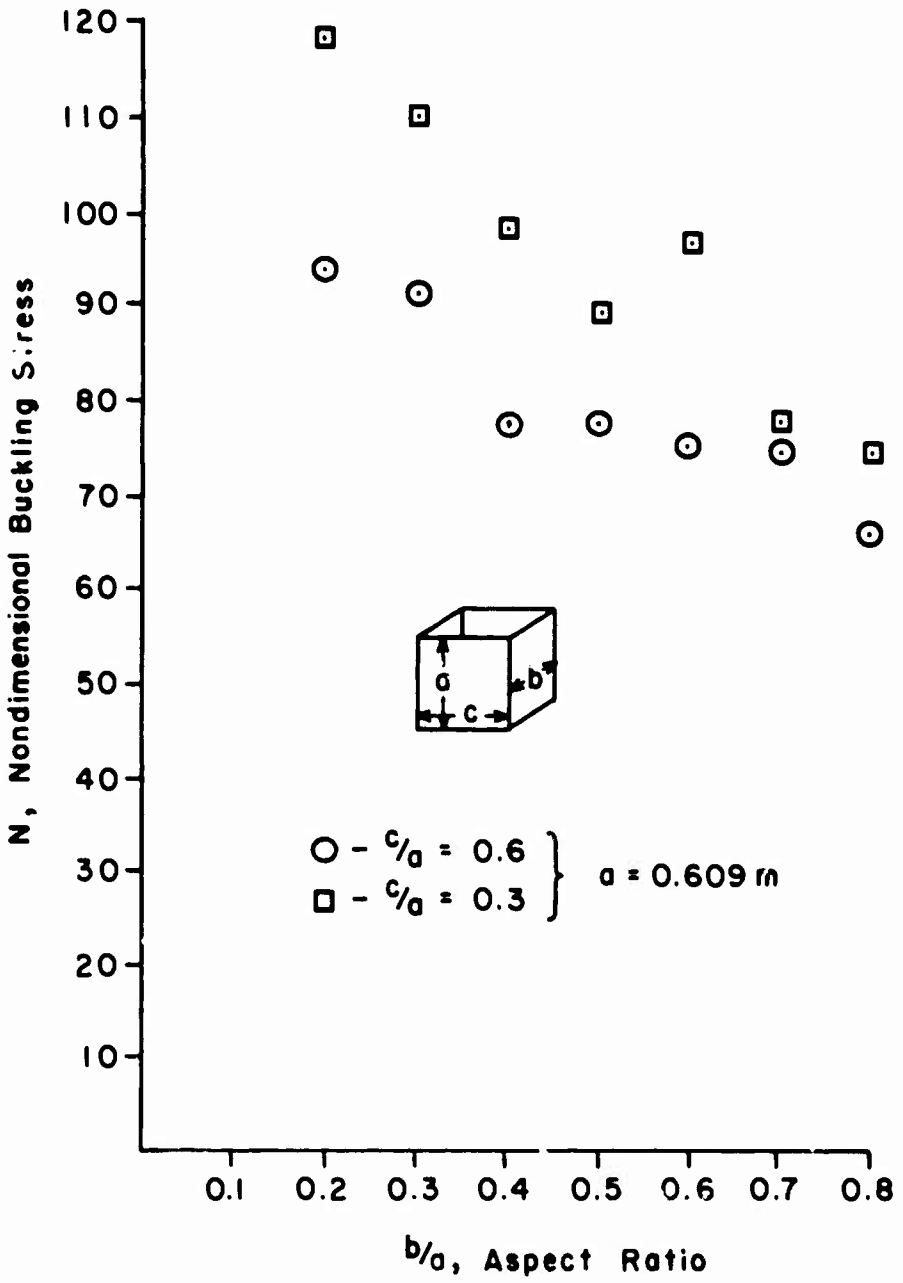

Figure 6 Experimental buckling stress as a function of aspect ratio

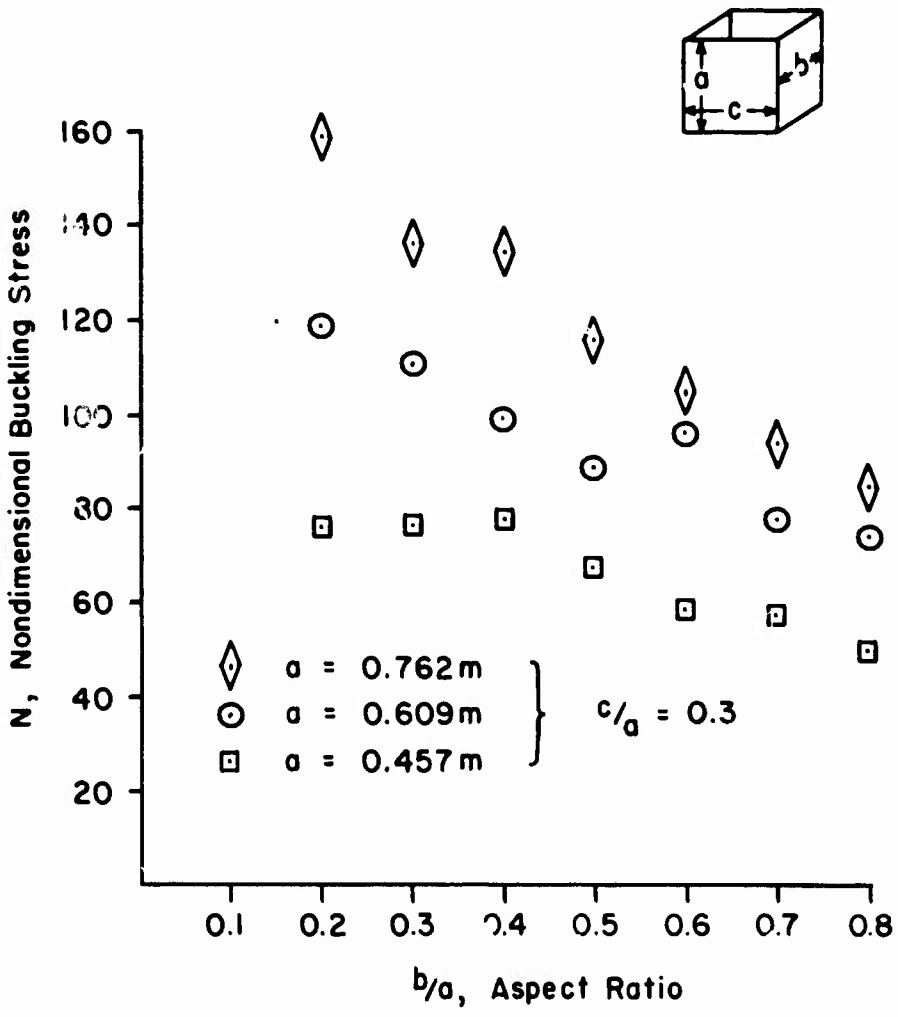

Figure 7 Experimental buckling stress as a function of aspect ratio and cylinder height

Theoretical Results and Comparison with Experiment

It will be recalled that solutions to the rectangular cylinder buckling problems were obtained for a uniform load by both exact and approximate techniques and for a nonuniform load by approximate techniques. The results of these solutions are shown in Figures 8 and 9, as plots of the nondimensional buckling load as a function of the aspect ratio. These results were obtained using the bending stiffness for V3C fiberboard given in reference 6. In Figure 8, which gives results for cylinders having the aspect ratio c/a = 0.6 with b/a as a variable ranging from 0.2 to 0.8, a comparison is shown of the exact solutions and the approximate solutions for the buckling stress. These solutions are everywhere within 5% of each other, which is sufficiently close to establish the validity of the approximate solution.

The experimental results are also shown on Figure 8. Comparison of these results with the theoretical predictions based on a uniform load indicates poor agreement. The theory has the proper trend of decreasing buckling stress with increasing aspect ratio, but the theory underestimates the buckling stress by as much as a factor of two. Thus the theoretical model using a uniform load does not give satisfactory results.

The results presented in reference 2 indicate the existence of a nonuniform load during buckling, and this seems reasonable when one considers the relatively greater stiffness of corner regions of the rectangular cylinder in comparison to that of the central regions of the sides. Being stiffer, the corners will support a greater portion of the load when the cylinder is subjected to a uniform compression or axial shortening which is the type of loading that occurred during the buckling tests. Because of this, solutions corresponding to the experimental results were obtained using the nonuniform load distribution specified in equation (29). It was not possible to obtain these solutions in a direct manner because this load distribution contains two unknowns, N, the average value of the buckling stress, and b_1, a parameter which determines the ratio of the maximum stress to the minimum stress. N will be determined as the eigenvalue of the solution but b_1 must be specified. For the results presented in Figures 8 and 9, b_1 was chosen so that the results were in fair agreement for one value of b/a and the same value of b_1 used for the remaining values of b/a. The values of b_1 used are given on the figures and are different for the two values of the aspect ratio c/a. Examination of the results presented in Figure 8 show that the predictions of the average buckling stress based on the described load distribution are in fair agreement with experimentally determined values of the buckling stress. The experimental values can also be considered as average values because they were computed by dividing the total buckling load by the perimeter of the cylinder. These comparisons between theory and experiment indicate that behavior can be characterized with a nonuniform load distribution. However, the exact form of this distribution is not known and cannot in an exact way be determined from the procedure developed here. This suggests treatment of the geometrically nonlinear buckling problem in which

the rectangular cylinder is subject to a uniform compression. The buckling stress distribution would be one of the results of this problem instead of a specified input.

This nonuniform load result also suggests an explanation of the unexpected variation of the nondimensional buckling stress with cylinder height found experimentally and discussed previously. The distribution of load, and thus stress, resulting from a uniform compressive deformation is dependent on the distribution of stiffness along perimeter of the cylinder. As indicated above, this distribution is influenced by the presence of the corners but it is also believed to be influenced by the height of the cylinder. For example; if compressive behavior predominates in the region near the corner and bending behavior in the central region of the sides, then the corner stiffness will vary inversely with cylinder height and the central stiffness inversely with the square of the cylinder height. As a result, as the height increases the stiffness of the corner will become more predominant resulting in a concentration of load at the corner with the resulting increase in the buckling strength with cylinder height. This mechanism provides behavior in agreement with experimental results and illustrates a possible explanation for the variation of buckling stress with cylinder height. It is believed that the true mechanism behind this behavior will be revealed by solution of the nonlinear buckling problem which includes the interaction of bending and compressive modes of deformation.

Figure 9 illustrates the behavior of the buckling stress as a function of the aspect ratio, b/a, with the other aspect ratio, c/a, equal to 0.3. The theoretical predictions from both the uniform and nonuniform load are considerably different in relation to the experimental results from that found for c/a = 0.6. For the present case, c/a = 0.3, the theoretical nonuniform load results are in fair agreement with the experimental results for $0.6 \leq b/a \leq 0.8$. For $b/a < 0.6$ the theoretical results are in poor agreement with large overprediction of the buckling stress. The phenomenon behind this behavior is suggested by the buckling behavior of flat plates subjected to stress beyond the elastic limit shown as an insert in Figure 9 and taken from reference 7. This data shows that as long as the buckling stress is below the yield stress, the classical buckling result holds; once the yield stress is reached, the plate will buckle regardless of size. The results for the rectangular cylinder shown on Figure 9 exhibit a similar behavior, taking the solution under nonuniform load as the classical buckling result and the experimental results as the branch representing the stability boundary due to plastic buckling. In this case buckling at a constant stress level is not observed because fiberboard does not have a sharply defined yield point, and the state of stress is not uniform as is the case in the example from reference 7. To further confirm the existence of plastic buckling in the experimental results, a measure of the level of the average stress, N, at which the stress in the rectangular cylinder reaches the yield point is needed. A convenient measure is provided by the maximum stress occurring in the nonuniform distribution used in this analysis. The value of N for which this maximum stress reached the yield point was computed and is plotted on Figure 9. As can be seen this value is in good agreement with the value at which

[7] S.P. Timoshenko and J.M. Gere; Therory of Elastic Stability; McGraw-Hill Book Company, 1961.

the experimental and theoretical results depart. Since this value of N is only a measure of the point at which plastic behavior begins, it is not surprising that the experimental results are greater. Thus it appears that in addition to the need for treatment of the geometrically nonlinear buckling problem, there is also a need to consider inelastic buckling in the case of rectangular cylinders with small aspect ratios.

These results have substantial impact on the selection and specification of fiberboard grades for a given packaging situation. This impact comes from the fact that for the buckling mode of failure the bending stiffness is the material property that determines package performance. That is, an increase in the bending stiffness gives a proportional increase in the buckling strength as shown by equation (2d). The present design and specification parameter for fiberboard is the Mullen burst strength, a property guide different from the bending stiffness. Thus it is recommended that the bending stiffness of fiberboard be used as an additional specification parameter. Such a parameter could be determined by simplification of the bending test procedure described in reference 6.

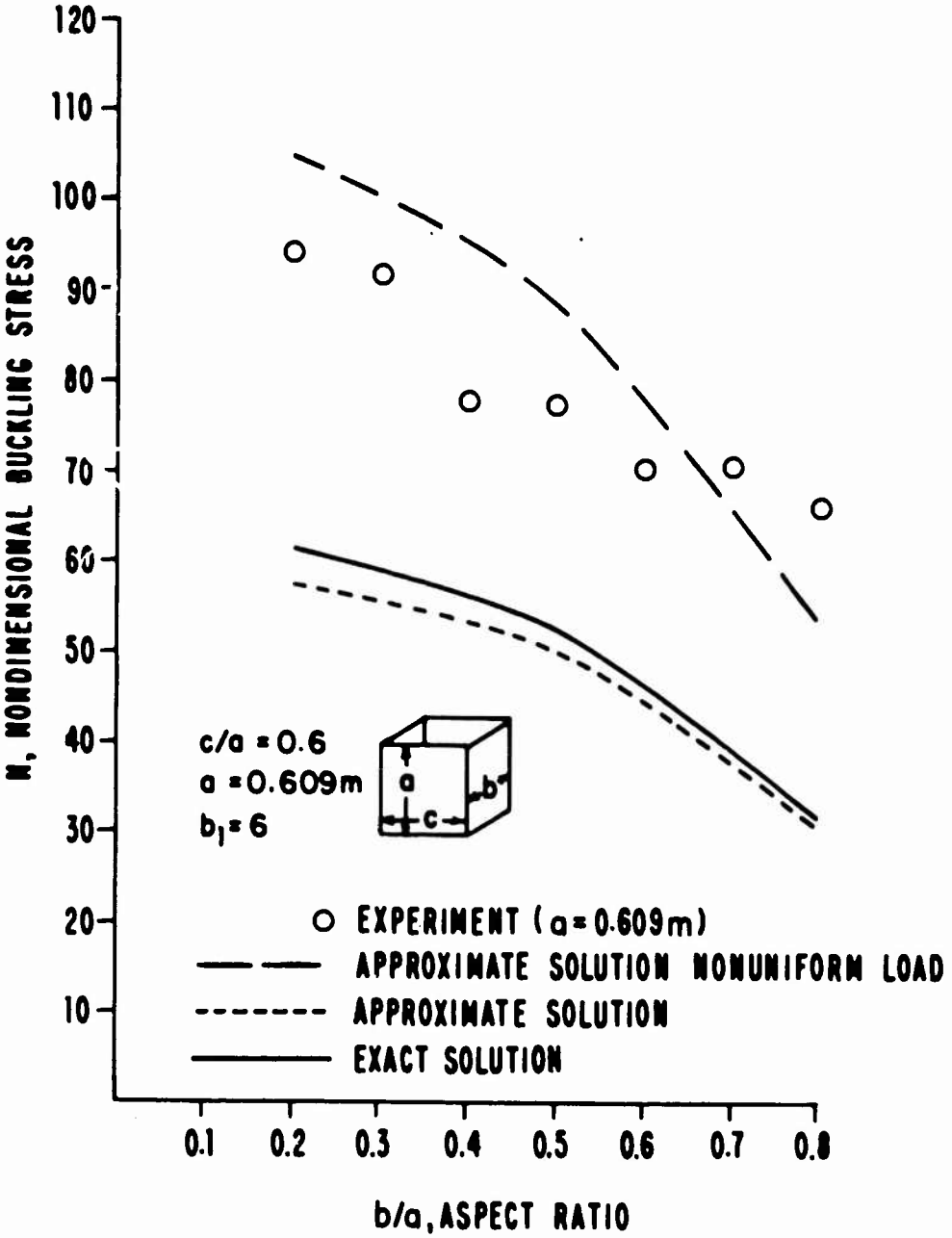

Figure 8 Theoretical predictions of the buckling stress and comparison with experiment

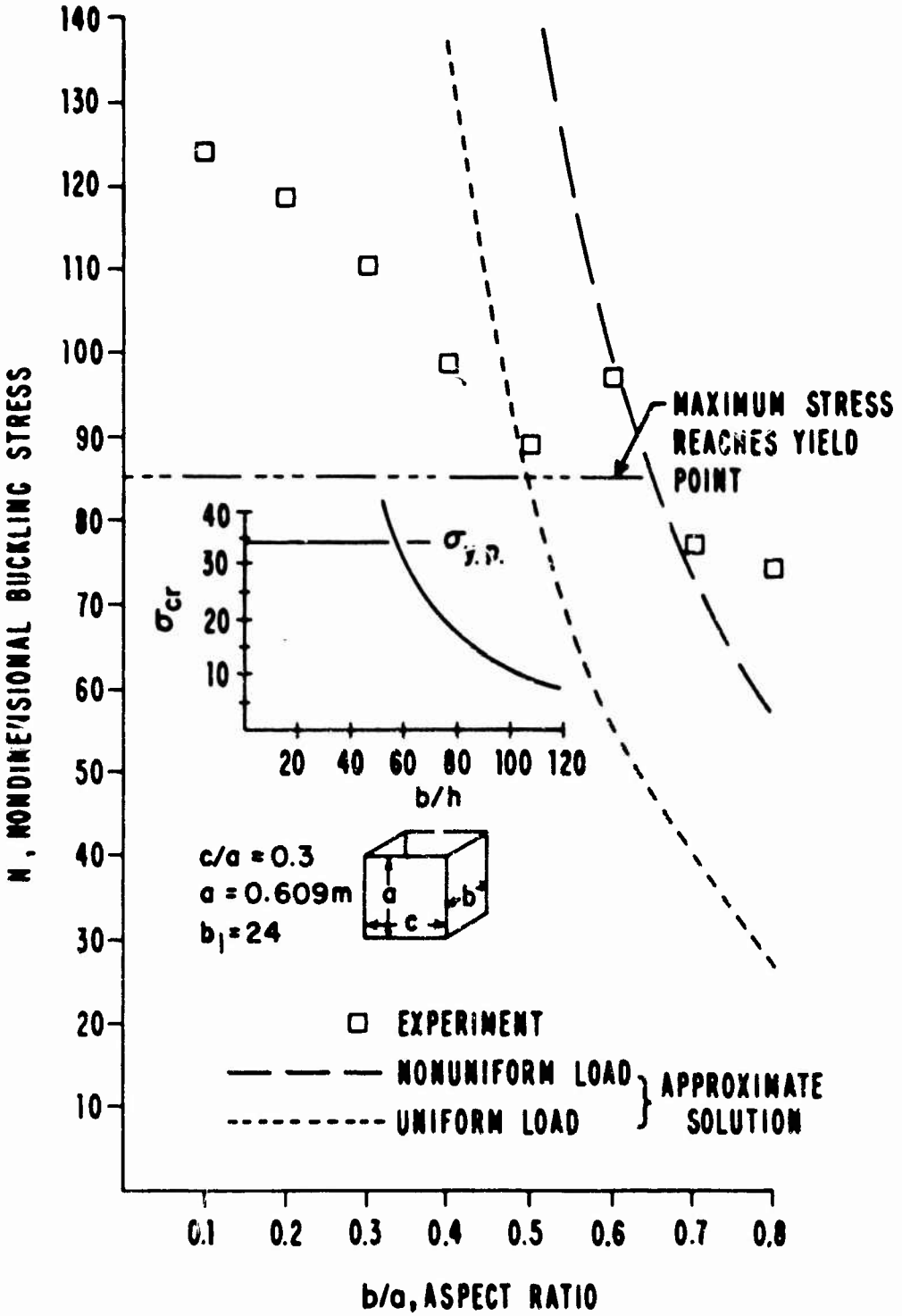

Figure 9 Theoretical prediction of the buckling stress and correlation with experiment

CONCLUSIONS

The results of a theoretical and experimental investigation of the buckling of rectangular cylinders has been presented. As a result of the comparison of the theoretical results with those determined experimentally, the following conclusions can be reached:

1. A theoretical model based on a uniform loading situation is inadequate for predicting the buckling stress of rectangular cylinders.

2. The classical buckling theory using a nonuniform load shows promising correlation with experimental results; however, with the classical theory it is not possible to completely determine the load distribution. To remedy this, the geometrically nonlinear buckling with a uniform compression or shortening of the cylinder should be studied.

3. For rectangular cylinders with small aspect ratios, inelastic buckling or material nonlinearity must be included in the theory to give adequate prediction of the buckling strength.

4. The bending stiffness should be used as an additional design and specification parameter for fiberboard used in packages and containers.

REFERENCES

1. Shick, P. E., and N. C. S. Chan; Top-to-Bottom Compression for Double Wall Corrugated Boxes: TAPPI Vol 48; No. 7; 1965; pp 423-430.

2. Angell, B. S. and P. R. Paslay; Determination of the Stacking Strength of Corrugated Fiberboard Containers; Proceedings of Society of Experimental Stress Analysis, Vol XVI, No. 1, pp 109-116.

3. Hearmon, R. F. S.; An Introduction to Applied Anisotropic Eleasticity; Oxford University Press; 1961.

4. Walton, W. C., Jr., and E. C. Steeves; A New Matrix Theorem and its Application for Establishing Independent Coordinates for Complex Dynamical Systems with Constraints, NASA TR R–326; 1969.

5. Walton, W. C., Jr.; Application of a General Finite Difference Method for Calculating Bending Deformations of Solid Plates, NASA TN D-536; 1960.

6. Steeves, E C; Orthotropic Bending Properties of Fiberboard; Technical Report 75-97-AMEL; U.S. Army Natick Development Center; 1975.

7. Timoshenko, S. P. and J. M. Gere; Theory of Elastic Stability; McGraw-Hill Book Company; 1961.

APPENDIX I

None vanishing elements of the matrix U

$$U_{11} = \beta \mathrm{Cos}\beta b/a + f_2 \alpha \mathrm{Cosh}\alpha b/a$$

$$U_{12} = \beta \mathrm{Sin}\beta b/a - f_1 \alpha \mathrm{Sinh}\alpha b/a$$

$$U_{13} = -\beta \mathrm{Cos}\beta c/a - f_4 \alpha \mathrm{Cosh}\alpha c/a$$

$$U_{14} = \beta \mathrm{Sin}\beta c/a - f_3 \alpha \mathrm{Sinh}\alpha c/a$$

$$U_{21} = -\beta^2 \mathrm{Sin}\beta b/a + f_2 \alpha^2 \mathrm{Sinh}\alpha b/a$$

$$U_{22} = \beta^2 \mathrm{Cos}\beta b/a - f_1 \alpha^2 \mathrm{Cosh}\alpha b/a$$

$$U_{23} = -\beta^2 \mathrm{Sin}\beta c/a + f_4 \alpha^2 \mathrm{Sinh}\alpha c/a$$

$$U_{24} = -\beta^2 \mathrm{Cos}\beta c/a + f_3 \alpha^2 \mathrm{Cosh}\alpha c/a$$

$$U_{33} = \beta \mathrm{Cos}\beta c/a + f_4 \alpha \mathrm{Cosh}\alpha c/a$$

$$U_{34} = \beta \mathrm{Sin}\beta c/a - f_3 \alpha \mathrm{Sinh}\alpha c/a$$

$$U_{35} = -\beta \mathrm{Cos}\beta b/a - f_2 \alpha \mathrm{Cosh}\alpha b/a$$

$$U_{36} = \beta \mathrm{Sin}\beta b/a - f_1 \alpha \mathrm{Sinh}\alpha b/a$$

$$U_{43} = -\beta^2 \mathrm{Sin}\beta c/a + f_4 \alpha^2 \mathrm{Sinh}\alpha c/a$$

$$U_{44} = \beta^2 \mathrm{Cos}\beta c/a - f_3 \alpha^2 \mathrm{Cosh}\alpha c/a$$

$$U_{45} = -\beta^2 \mathrm{Sin}\beta b/a + f_2 \alpha^2 \mathrm{Sinh}\alpha b/a$$

$$U_{46} = -\beta^2 \mathrm{Cos}\beta b/a + f_1 \alpha^2 \mathrm{Cosh}\alpha b/a$$

$$U_{55} = \beta \mathrm{Cos}\beta b/a + f_2 \alpha \mathrm{Cosh}\alpha b/a$$

$$U_{56} = \beta \mathrm{Sin}\beta b/a - f_1 \alpha \mathrm{Sinh}\alpha b/a$$

APPENDIX I
(cont'd)

$$U_{57} = -\beta \mathrm{Cos}\beta c/a - f_4 \alpha \mathrm{Cosh}\alpha c/a$$

$$U_{58} = \beta \mathrm{Sin}\beta c/a - f_3 \alpha \mathrm{Sinh}\alpha c/a$$

$$U_{65} = -\beta^2 \mathrm{Sin}\beta b/a + f_2 \alpha^2 \mathrm{Sinh}\alpha b/a$$

$$U_{66} = \beta^2 \mathrm{Cos}\beta b/a - f_1 \alpha^2 \mathrm{Cosh}\alpha b/a$$

$$U_{67} = -\beta^2 \mathrm{Sin}\beta c/a + f_4 \alpha^2 \mathrm{Sinh}\alpha c/a$$

$$U_{68} = -\beta^2 \mathrm{Cos}\beta c/a + f_3 \alpha^2 \mathrm{Cosh}\alpha c/a$$

$$U_{71} = -\beta \mathrm{Cos}\beta b/a - f_2 \alpha \mathrm{Cosh}\alpha b/a$$

$$U_{72} = \beta \mathrm{Sin}\beta b/a - f_1 \alpha \mathrm{Sinh}\alpha b/a$$

$$U_{77} = \beta \mathrm{Cos}\beta c/a + f_4 \alpha \mathrm{Cosh}\alpha c/a$$

$$U_{78} = \beta \mathrm{Sin}\beta c/a - f_3 \alpha \mathrm{Sinh}\alpha c/a$$

$$U_{81} = -\beta^2 \mathrm{Sin}\beta b/a + f_2 \alpha^2 \mathrm{Sinh}\alpha b/a$$

$$U_{82} = -\beta^2 \mathrm{Cos}\beta b/a + f_1 \alpha^2 \mathrm{Cosh}\alpha b/a$$

$$U_{87} = -\beta^2 \mathrm{Sin}\beta c/a + f_4 \alpha^2 \mathrm{Sinh}\alpha c/a$$

$$U_{88} = \beta^2 \mathrm{Cos}\beta c/a + f_3 \alpha^2 \mathrm{Cosh}\alpha c/a$$

APPENDIX II

$$a_1 = 1/2\left[e_2/\Delta\eta_1^4 + e_4(n\pi)^2/\Delta\eta_1^2\right]$$

$$a_2 = 1/2\left[-e_3(n\pi)^2/\Delta\eta_1^2 - 2e_2/\Delta\eta_1^4\right]$$

$$a_3 = 1/2\left[e_2/\Delta\eta_1^4 - e_4(n\pi)^2/\Delta\eta_1^2\right]$$

$$a_4 = 1/2\left[(n\pi)^4 + 4e_3(n\pi)^2/\Delta\eta_1^2 + 4e_2/\Delta\eta_1^4\right]$$

$$a_5 = 1/2\left[-e_3(n\pi)^2/\Delta\eta_1^2 - 2e_2/\Delta\eta_1^4\right]$$

$$a_6 = 1/2\left[e_2/\Delta\eta_1^4 + e_4(n\pi)^2/\Delta\eta_1^2\right]$$

$d_i = 1/2\,(n\pi)^2$ uniform buckling stress

$\Delta\eta_1 \rightarrow \Delta\eta_2$ where applicable

$$d_i = \begin{cases} 1 + b_1 \dfrac{(c/a)^2}{(b/a)^2}\left[(\eta_{1i} - \dfrac{b}{a})^2\right] - \dfrac{1}{3}\left(\dfrac{b}{a}\right)^2\right] & 0 \leq \eta_1 \leq \dfrac{b}{a} \\ 1 + b_1\left[(\eta_{2i} - \dfrac{c}{a})^2 - \dfrac{1}{3}\left(\dfrac{c}{a}\right)^2\right] & 0 \leq \eta_2 \leq \dfrac{c}{a} \end{cases}$$

nonuniform buckling stress

APPENDIX III

Non-vanishing element of the constraint matrix.

$C(1,2) = 1.0$

$C(2, m+3) = 1.0$

$C(3,3) = 1/2\Delta\eta_1$

$C(3,1) = -1/2\Delta\eta_1$

$C(3, m+4) = -1/2\Delta\eta_2$

$C(3, m+2) = 1/2\Delta\eta_2$

$C(4,1) = 1/\Delta\eta_1^2$

$C(4,2) = -2/\Delta\eta_1^2$

$C(4,3) = 1/\Delta\eta_1^2$

$C(4, m+2) = 1/\Delta\eta_2^2$

$C(4, m+3) = -2/\Delta\eta_2^2$

$C(4, m+4) = 1/\Delta\eta_2^2$

$C(5, 2m+3) = 1$

$C(5, m) = -1$

$C(6, 2m+4) = 1$

$C(6, 2m+1) = -1$

LIST OF SYMBOLS

a	Cylinder height
a_i	Stiffness matrix constants
A_i, B_i, C_i, D_i	Constants of integration
b, c	Cylinder side widths
b_i	A constant used to describe the nonuniform buckling load
d_i	Buckling load matrix constant
D_{jk}	Bending stiffness constants
e_1, e_2, e_3, e_4	Bending stiffness ratios
E	Energy density function
f_i	Constants defined by equation 10
$F_i(\eta_i)$	Function describing the normal displacement
m	Number of grid points per side
n	Axial half-wave number
N_x	Axial stress resultant
N	Nondimensional axial stress resultant
$\bar{N}$	Average value of N
P	Product of eigenvalues
w_i	Normal displacement of the ith side of cylinder
x, y_i	Position coordinates on the ith side of cylinder
α, β	Characteristic numbers defined by equation 6
ξ, η_i	Nondimensional coordinates corresponding with (x, y_i)

LIST OF SYMBOLS (cont'd)

Matrices

$[C]$	Constraint matrix
$[Q]$	Matrix of eigenvectors $\{q\}$
$[S]$	Stiffness matrix associated with $\{w\}$
$[\bar{S}]$	Stiffness matrix associated with $\{q\}$
$[T]$	Buckling load matrix associated with $\{w\}$
$[\bar{T}]$	Buckling load matrix associated with $\{q\}$
$[U]$	Boundary condition matrix
$[\beta]$	Matrix defining the generalized coordinates

Vectors

$\{c\}$	Vector of integration constants
$\{w\}$	Vector of finite difference grid point displacements
$\{q\}$	Vector of generalized coordinates defined by equation (5)